Article

THE KINEMATIC SIGNATURE OF FACE-ON PEANUT-SHAPED BULGES

Debattista, Victor P, Carollo, Marcella C, Mayer, Lucio and oore, Ben

Debattista, Victor P orcid iconORCID: 0000-0001-7902-0116, Carollo, Marcella C, Mayer, Lucio and oore, Ben (2005) THE KINEMATIC SIGNATURE OF FACE-ON PEANUT-SHAPED BULGES. The Astrophysical Journal, 628 . pp. 678-694. ISSN 0004-637X

The Astrophysical Journal, 628:678–694, 2005 August 1

THE KINEMATIC SIGNATURE OF FACE-ON PEANUT-SHAPED BULGES

Victor P. Debattista[1,2] and C. Marcella Carollo
Institut für Astronomie, ETH Zürich, CH-8093 Zurich, Switzerland; debattis@astro.washington.edu, marcella.carollo@phys.ethz.ch

and

Lucio Mayer and Ben Moore
Department of Theoretical Physics, University of Zürich, Winterthurerstrasse 190, CH-8057 Zurich, Switzerland; lucio@physik.unizh.ch, moore@physik.unizh.ch
Received 2005 January 10; accepted 2005 April 20

ABSTRACT

We present a kinematic diagnostic for peanut-shaped bulges in nearly face-on galaxies. The face-on view provides a novel perspective on peanuts that would allow study of their relation to bars and disks in greater detail than hitherto possible. The diagnostic is based on the fact that peanut shapes are associated with a flat density distribution in the vertical direction. We show that the kinematic signature corresponding to such a distribution is a minimum in the fourth-order Gauss-Hermite moment s_4. We demonstrate our method on *N*-body simulations of varying peanut strength, showing that strong peanuts can be recognized to inclinations $i \simeq 30^\circ$, regardless of the strength of the bar. We also consider compound systems in which a bulge is present in the initial conditions, as may happen if bulges form at high redshift through mergers. We show that in this case, because the vertical structure of the bulge is not derived from that of the disk, the signature of a peanut in s_4 is weakened. Thus the same kinematic signature of peanuts can be used to explore bulge formation mechanisms. The observational requirements for identifying peanuts with this method are challenging, but feasible.

Subject headings: galaxies: bulges — galaxies: evolution — galaxies: formation — galaxies: kinematics and dynamics — galaxies: photometry — galaxies: spiral

Online material: mpeg animations

1. INTRODUCTION

About 25% of the stellar luminosity in the universe comes from the bulges of disk galaxies (Persic & Salucci 1992; Fukugita et al. 1998). Therefore, understanding how bulges form is a necessary step in understanding galaxy formation in general.

If bulges are distinct entities, rather than just disk light in excess of an exponential (van den Bosch et al. 2002; Böker et al. 2003), a mechanism for generating them separate from disk formation must be considered. Because bulges sit at the bottom of the potential wells of galaxies, many paths for their formation are possible. Bulge formation scenarios can be classified loosely based on whether the driving mechanism is internal or external. A widely discussed example of externally driven bulge formation is in the merger at early times of dwarf-sized galactic subunits around which disks subsequently grow (Kauffmann et al. 1993). Observational evidence supporting this scenario includes the relatively homogeneous bulge stellar populations in the Milky Way (Ferreras et al. 2003; Zoccali et al. 2003) and Andromeda (Stephens et al. 2003), and counterrotation found in some galaxies (Pizzella et al. 2004).

Discussion of internally driven bulge formation has focused on the secular evolution of disk instabilities. Observational evidence supporting secular bulge formation includes disklike, almost-exponential light profiles (Andredakis & Sanders 1994; Courteau et al. 1996; de Jong 1996; Carollo et al. 1998, 2001; Carollo 1999; MacArthur et al. 2003), occasionally disklike, cold kinematics (Kormendy 1993; Kormendy et al. 2002), the correlation between the scale lengths of bulges and disks (de Jong 1996; MacArthur et al. 2003), and the similar average colors of bulges and inner disks (Terndrup et al. 1994; Peletier & Balcells 1996; Courteau et al. 1996). The recent review of Kormendy & Kennicutt (2004) summarizes our current understanding of, and evidence for, secular formation of some bulges.

The bulges of many edge-on galaxies are box- or peanut- (B/P) shaped (Burbidge & Burbidge 1959; Jarvis 1986). Binney & Petrou (1985) constructed axisymmetric models of B/P bulge systems, including cylindrical rotation as observed by Kormendy & Illingworth (1982). They speculated that accretion is responsible for creating such systems; however, observations found little evidence of accretion onto them (Shaw 1987; Whitmore & Bell 1988; but see also Lütticke et al. 2004). A different scenario emerged from three-dimensional *N*-body simulations, namely, formation via secular evolution of bars (Combes & Sanders 1981), either through resonant scattering or through bending instabilities (Pfenniger 1984; Combes et al. 1990; Pfenniger & Friedli 1991; Raha et al. 1991). The orbits supporting peanuts have been studied extensively (Combes et al. 1990; Pfenniger 1984, 1985; Patsis et al. 2002b) and shown to generally arise from vertically unstable x_1 orbits. Patsis et al. (2002b) showed that these orbits are present and peanuts are possible even if the nonaxisymmetric perturbation is very weak.

Thereafter, observational efforts sought to establish the connection between B/P-shaped bulges and bars by seeking evidence for a bar in edge-on B/P-bulged systems. In the case of NGC 4442, the B/P bulge is already apparent at an inclination of 72°, at which the bar also can be recognized (Bettoni & Galletta

[1] Current address: Astronomy Department, University of Washington, Box 351580, Seattle, WA 98195.
[2] Brooks Fellow.

1994). A second such case is NGC 7582 at an inclination of 65° (Quillen et al. 1997). In several B/P bulges, photometric features of a bar have been claimed (e.g., de Carvalho & da Costa 1987), but the bar interpretation is not unique when only photometry is available. The fraction of edge-on bulges having B/P shapes is ~45% (Lütticke et al. 2000), which is consistent with the fraction of galaxies containing bars (~70%; Knapen et al. 2000; Eskridge et al. 2000), once the arbitrary orientations of bars to the line of sight (LOS) are considered. However, the most important evidence for the presence of bars in B/P bulges comes from a comparison of the edge-on gas and stellar LOS velocity distributions (LOSVDs) of *N*-body bars (Bureau & Athanassoula 1999, 2005; Athanassoula & Bureau 1999) and real galaxies (Kuijken & Merrifield 1995; Merrifield & Kuijken 1999; Bureau & Freeman 1999; Chung & Bureau 2004).

These edge-on studies have established the connection between B/P-shaped bulges and bars. However, the degeneracy inherent in deprojecting edge-on galaxies makes it difficult to study other properties of the host galaxy. Moreover, while B/P shapes are produced by bars, this does not exclude the possibility that bulges are *shaped* by secular processes, not formed by them. Addressing this issue requires an attempt at a cleaner separation of bulges, bars, and peanuts. In face-on systems the viewing geometry is well constrained and bars are readily apparent. If we can also recognize peanuts in them, then we obtain an important new perspective on the relation of peanuts and bars. For example, this permits study of the relative sizes of bars and peanuts: meager observational evidence suggests that these need not be equal (Kormendy & Kennicutt 2004), in agreement with simulations (below). Moreover, for inclinations of ~30°, it becomes possible to measure accurately the pattern speed of the bar (Debattista 2003) and therefore to test for resonances and compare with theoretical predictions. It would also allow determination of the fraction of barred galaxies with peanuts, which may be different from the fraction of peanuts with bars. And finally, as we show below, the ability to detect peanuts face-on opens the possibility of exploring bulge formation mechanisms.

In this paper we examine the kinematic signature of peanuts in face-on galaxies. In § 2 we first explore some simple analytic models to help understand the behavior of more realistic systems. Working with Gauss-Hermite moments (Gerhard 1993; van der Marel & Franx 1993), we show that the fourth-order LOSVD moment, s_4, is monotonically increasing with d_4, the fourth-order vertical density moment. Thus s_4 can be used to probe the vertical structure of a disk. We describe the *N*-body building in § 3, and in § 4 we present the *N*-body models, with and without strong peanuts, used in this paper and examine their vertical density distributions. We show that the main signature of a peanut is in d_4, rather than in the disk scale height. We explore the vertical LOSVDs of these *N*-body models in § 5, showing that s_4 can be used as a robust kinematic signature of a peanut, independent of bar strength. In § 6 we show that moderate inclinations do not substantially degrade the diagnostic. Section 7 discusses the required signal-to-noise ratio (S/N) and spectral resolution, and our conclusions are presented in § 8.

2. EXACT RESULTS

We first consider some exact models useful for interpreting the results of *N*-body simulations. Peanuts constitute a density distribution more vertically extended than the surrounding disk. Let us denote the root mean square (rms) height and vertical velocity as h_z and σ_z, respectively. Deviations from Gaussian distributions can be parameterized by the moments of an expansion in Gauss-Hermite functions (Gerhard 1993; van der Marel & Franx 1993). The second-order term in such an expansion is related to the rms. The third-order term measures deviations that are asymmetric about the mean and are therefore likely to be small for the vertical density and velocity distributions of disk galaxies. The fourth-order term measures the lowest order symmetric deviation from a Gaussian; it is negative when a distribution is broader than Gaussian and positive when it is more peaked. We denote the fourth-order Gauss-Hermite moment of the vertical density distribution as d_4 and that for the LOSVD as s_4. Following Gerhard (1993), for a vertical LOSVD $l(v_z)$ normalized to the projected surface density Σ, we define

$$s_4 = \frac{\sqrt{4\pi}}{\Sigma} \int l(w) H_4(w) e^{-(1/2)w^2} dw, \tag{1}$$

where $w = (v_z - \bar{v}_z)/\sigma_z$ and $H_4(w) = [1/(768\pi)^{1/2}](16w^6 - 48w^2 + 12)$. A similar expression holds for d_4. For a particle model, the integral becomes a sum and Σ is replaced by N_p, the number of particles in a bin.

The vertical density extension associated with the peanut will correspond to an increase in h_z (the "scale height") and/or a decrease in d_4. What is the observable effect on the LOSVD of such variations? First consider how σ_z varies as a function of radius in the case where h_z is constant. In a single-component axisymmetric system, the one-dimensional vertical Boltzmann+ Poisson equation is

$$\frac{\partial}{\partial z}\left(\frac{1}{\rho}\frac{\partial}{\partial z}\rho\bar{v}_z^2\right) = -4\pi G\rho \tag{2}$$

(e.g., Binney & Tremaine 1987, eq. [4-38]). If the system is isothermal, then $\bar{v}_z^2$ is independent of z (and is therefore equal to σ_z^2). The solution of equation (2) is

$$\rho(z) = \rho_0 \mathrm{sech}^2(z/z_0) \tag{3}$$

(Spitzer 1942), where ρ_0 is the density in the mid-plane and

$$z_0 = \frac{\sigma_z}{\sqrt{2\pi G\rho_0}} = \frac{\sigma_z^2}{\pi G\Sigma}. \tag{4}$$

[Note that for the isothermal disk, $h_z = z_0\pi/(12)^{1/2}$.] Thus if z_0 is (nearly) constant (as suggested by observations [van der Kruit & Searle 1981; de Grijs & Peletier 1997]), then $\sigma_z^2 \propto \Sigma$. Since typically $\Sigma(R) \propto e^{-R/R_d}$, then $\sigma_z \propto e^{-R/2R_d}$ and it is likely that any signature of the peanut in σ_z will be swamped by this density-driven radial variation.

Next we use simple models to explore the signature in the LOSVD of a flat-topped vertical density distribution. Consider Camm's (1950) series of analytic solutions of the collisionless Boltzmann equation for systems stratified in plane-parallel layers of infinite extent. This is a good local approximation to real galaxies at low z when the rotation curve is flat (van der Kruit & Freeman 1986). In Camm's model III, the density distribution is given by $\rho(z) = \rho_0 \cos^{2-2/n}\theta$, where $n > 3/2$ and the parameter θ is defined by the relation

$$z = A \int_0^\theta \sec^{1-2/n}\phi \, d\phi, \tag{5}$$

with A some constant. Several examples of this density distribution for different n are presented in Figure 1. The corresponding distribution function is

$$f(w,\theta) = C(n)(2n\cos^{2/n}\theta - w^2)^{n-3/2}, \tag{6}$$

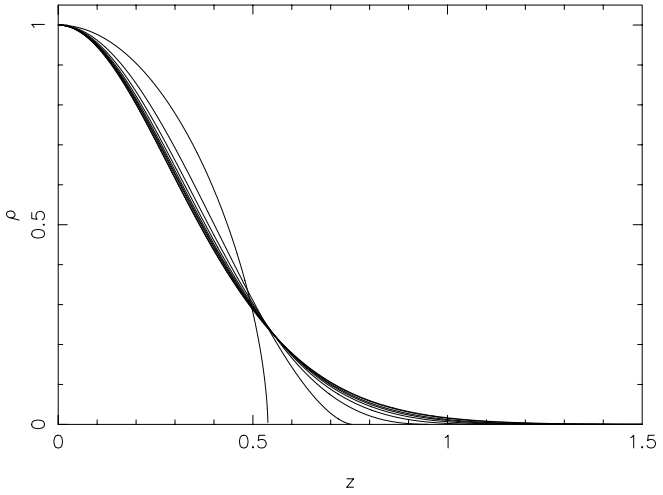

FIG. 1.—Model III of Camm (1950). Various vertical density profiles, with n increasing in order of increasing maximum z, from $n = 1.6$ in steps of 1, are shown.

where $C(n)$ is a normalization constant. These densities and distribution functions can be integrated numerically to compute d_4 and s_4. The results are presented in Figure 2. The limit $n \to \infty$ corresponds to the isothermal sheet, in which the distribution function has the same Gaussian dependence on velocity at all heights. Thus in this limit, $s_4 = 0$. On the other hand, the isothermal sheet has a $\mathrm{sech}^2 z$ profile that is more peaked than a Gaussian and therefore has $d_4 > 0$. At smaller n, the density profile becomes increasingly flat-topped, leading to $d_4 < 0$, which drives $s_4 < 0$. Two properties of s_4 make it an excellent probe of d_4. First is the fact that s_4 increases monotonically with d_4, which makes s_4 an observable surrogate for the unobservable d_4. Second, $s_4 \lesssim d_4$, so that the vertical velocity distribution is generally broader than the density distribution, which makes it observationally robust.

3. *N*-BODY SYSTEMS

We use N-body models with different initial conditions and evolved on different codes to study the kinematic signatures of face-on peanuts. Since gas is generally depleted within bars and, moreover, dissipates its vertical energy, it is not a good tracer of face-on peanuts. We therefore focus on only the stellar kinematics of peanuts, and our simulations are all collisionless. Table 1 lists all the simulations used in this study.

3.1. *Rigid-Halo Simulations*

The highest resolution simulations in this paper were run on a three-dimensional cylindrical particle-mesh (PM) grid code (described in Sellwood & Valluri 1997). The main advantages of this code for the present study are that it permits high spatial and mass resolutions; indeed, these simulations used $\geq$4 million disk particles and force softening $\epsilon \leq 2z_d/3$, where z_d is the (constant) Gaussian vertical scale height of the initial conditions. Since Gauss-Hermite moments generally require high S/Ns to be measured reliably, a large number of particles is desirable. At the same time, the high force resolution ensures that the vertical motions of particles are well resolved.

The rigid halos were represented by either a spherical logarithmic potential,

$$\Phi_L(r) = \frac{v_h^2}{2} \ln\left(r^2 + r_h^2\right), \tag{7}$$

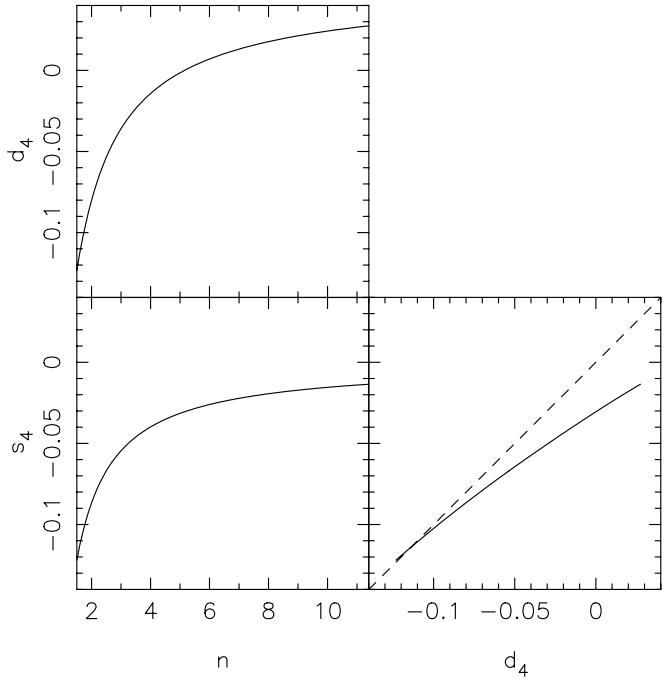

FIG. 2.—Gauss-Hermite moments d_4 and s_4 of model III of Camm (1950). The left panels show the variation of these parameters with n, while the panel on the right plots s_4 vs. d_4. The dashed diagonal line indicates $s_4 = d_4$.

or a Hernquist (1990) model,

$$\Phi_{\mathrm{H}}(r) = -\frac{M_h}{r + r_h}, \tag{8}$$

where r_h is a halo scale radius, v_h is a characteristic halo velocity, and M_h is a halo mass. We define $v_h \equiv (GM_h/r_h)^{1/2}$ for the Hernquist halos.

The initially axisymmetric disks were all Sérsic type

$$\rho_d(R,z) \propto (1 - f_b) M e^{-(R/R_d)^{1/n}} e^{-(1/2)(z/z_d)^2}, \tag{9}$$

where f_b is the fraction of the active (i.e., bulge+disk) mass that is in the bulge, M is the active mass, R_d is the disk scale length, z_d is the Gaussian thickness, and n is the Sérsic index ($n = 1$ corresponding to an exponential profile and $n = 4$ to a de Vaucouleurs profile). Disk kinematic setup used the epicyclic approximation with constant Toomre Q and the vertical Jeans equation to set vertical motions appropriate for a constant Gaussian thickness. We use units where $R_d = M = G = 1$, which gives a unit of time $(R_d^3/GM)^{1/2}$.

Bulges were generated using the method of Prendergast & Tomer (1970), where a distribution function is integrated iteratively in the global potential until convergence. We used the isotropic distribution function of a lowered polytrope, truncated at r_b,

$$f(\boldsymbol{x}, \boldsymbol{v}) \propto \left[-E(\boldsymbol{x}, \boldsymbol{v})\right]^{1/2} - \left(-E_{\max}\right)^{1/2}. \tag{10}$$

Here $E_{\max} = \Phi_{\mathrm{tot}}(r_b)$, the total potential at r_b in the disk plane. For all bulges we set $r_b = 0.78$. The bulges in runs B2 and B3 were fully rotating, while that in run B1 had no rotation. Further details of the compound system setup method used can be found in Debattista & Sellwood (2000).

TABLE 1
THE SAMPLE OF SIMULATIONS USED IN THIS PAPER

Run	N_* (10^6)	n	R_d/ϵ	z_d/ϵ	Q	f_b	Halo	r_h	v_h	Peanut
R1	7.5	1.0	60	3.0	1.2	0.0	Log	3.3	0.68	Strong
R2	7.5	1.0	60	6.0	1.2	0.0	Log	3.3	0.68	Strong
R3	4.0	1.0	60	3.0	2.4	0.0	Hern	20.8	1.44	Strong
R4	7.5	2.5	60	3.0	1.0	0.0	Log	3.3	0.68	Strong
R5	7.5	1.0	60	6.0	2.4	0.0	Log	3.3	0.68	Weak
R6	7.5	1.0	60	12.0	1.2	0.0	Log	3.3	0.68	None
R7	4.0	1.0	60	3.0	1.6	0.0	Hern	20.8	1.44	None
R8	7.5	1.0	60	3.0	1.2	0.0	Log	3.3	0.68	None
B1	4.0	1.0	80	8.0	2.5	0.2	Log	5.0	0.65	Weak
B2	4.0	1.0	80	8.0	1.9	0.2	Log	5.0	0.65	Strong
B3	4.0	1.0	80	8.0	1.3	0.2	Log	5.0	0.65	Strong
L1	0.2	1.0	40	6.0	0.0	0.0	NFW	108	76	Strong

NOTES.—N_* is the number of disk+bulge particles, n is the index of the initial Sérsic disk, R_d, z_d, and ϵ are the scale length and scale height of the *initial* disk and the softening length, Q is the initial-disk Toomre Q, and f_b is the bulge mass as a fraction of the total (disk+bulge). In the "Halo" column we describe the type of halo used: logarithmic, Hernquist, or NFW. The terms r_h and v_h are the halo scale length and characteristic velocity, respectively. In the "Peanut" column we give a qualitative description of the peanut: strong, weak, or none. For the live-halo system L1, we give the minimum Q, z_d is for a sech^2 profile, and $r_h = r_{\rm vir}$ and $v_h = V_{\rm vir}$ in kpc and km s^{-1}, respectively.

The polar grids were $N_R \times N_\phi \times N_z = 60 \times 64 \times 225$ or larger. For all the PM simulations, the vertical spacing of the grid planes, δz, was set to 0.0125. We used Fourier terms up to $m = 8$ in the potential, which was softened with the standard Plummer kernel. Time integration was performed with a leapfrog integrator with a fixed time step, $\delta t = 0.02$ for simulations B1–B3, $\delta t = 0.0025$ for run R4, and $\delta t = 0.01$ for all the rest.

3.2. *Live-Halo Simulation*

The disadvantage of the PM code is that we needed to use a rigid halo. Therefore in run L1 we used a lower mass resolution live-halo simulation run with PKDGRAV (Stadel 2001), a multistepping, parallel tree code.

The live-halo model was built using the technique developed by Hernquist (1993; see also Springel & White 1999). We start with an isotropic NFW halo (Navarro, Frenk, & White 1996) with virial radius $R_{\rm vir} = 108$ kpc, circular velocity at the virial radius $V_{\rm vir} = 76$ km s^{-1}, and virial mass $M_{\rm vir} = 1.5 \times 10^{11}\, M_\odot$. Then adiabatic contraction of the halo due to the presence of the disk is taken into account assuming that the spherical symmetry of the halo is retained and that the angular momentum of individual dark matter orbits is conserved (see Springel & White 1999). The disk mass fraction relative to the halo virial mass $f_d = M_d/M_{\rm vir} = 0.08$. We used an exponential disk with scale length $R_d = 1.99$ kpc and a sech$^2(z/z_d)$ vertical profile. We set $z_d = 0.15R_d$ and softening length $\epsilon = 50$ pc. The velocity field of the disk was calculated as in Springel & White (1999), assuming that the radial and vertical velocity dispersions are equal, $\sigma_R = \sigma_z$, with σ_R chosen to give a minimum Toomre $Q = 1.2$. Then the azimuthal velocity dispersion is determined from σ_R using the epicyclic approximation.

4. VERTICAL DENSITY OF THE *N*-BODY MODELS

The evolution of model B1 has been described in Debattista (2003), while runs B2 and B3 formed part of the preliminary survey for the Milky Way modeling described in Bissantz et al. (2004). The evolution of most of the remaining models will be described elsewhere (V. P. Debattista et al. 2005, in preparation). Here we are interested primarily in the final systems, not in details of their evolution. Except for run R3, which formed only a very weak oval distortion, all these simulations formed bars. The edge-on view of simulations R1–R8 is presented in Figure 3. Throughout this paper, we use a convention where the bar is along the x-axis and the z-axis is perpendicular to the disk. Runs R1–R4 contain prominent peanuts that were produced by bending instabilities (Raha et al. 1991; Merritt & Sellwood 1994). To better present these peanuts, in Figure 4 we present the edge-on projected density of particles in the narrow range $-0.5 \le y \le 0.5$; i.e., we show only a narrow slice of each model extending to about the minor axis of the bar. This gives a better appreciation of the peanuts that will be sought in the face-on view, where the disks do not mask peanuts. Peanuts can form in weakly barred systems (Patsis et al. 2002a); the peanut in run R3 formed in the presence of only a very weak oval. As a result, this peanut is almost axisymmetric. Run R5 contains a weak peanut while runs R6–R8 have no peanuts at all. Run R8 is identical to run R1 except for one important detail: we forced symmetry about the mid-plane. Therefore, although the velocity ellipsoid is very anisotropic with $\sigma_z/\sigma_R \simeq 0.25$ through most of the bar, the system could not bend and did not develop a peanut.

Comparing the peanuts visible in Figures 3 and 4 with the bars seen in the face-on surface density overlaid on Figure 5, it is apparent that the peanut in run R1 is smaller than the bar. Kormendy & Kennicutt (2004) noted that the peanut in the moderately inclined galaxy NGC 7582 was significantly shorter than the bar, and worried that this may be a problem for a secular peanut formation scenario. Run R1 shows that peanuts need not fill the entire major axis of a bar (see also Athanassoula 2005). In contrast, the peanut in run R2 extends to about the ends of the bar.

Figure 5 shows maps of h_z for runs R1–R8. On the bar's major axis h_z increases radially outward, reaching a maximum when a peanut is present. In most cases, the local maximum in h_z occurs close to the peanut. On the other hand, in runs R6–R8, none of which contain a peanut, h_z increases throughout.

The maps in Figure 6 show d_4 for runs R1–R8. Minima in d_4 correlate well with the location of peanuts, and there are no significant minima in d_4 other than at $R = 0$ in the absence of a peanut.

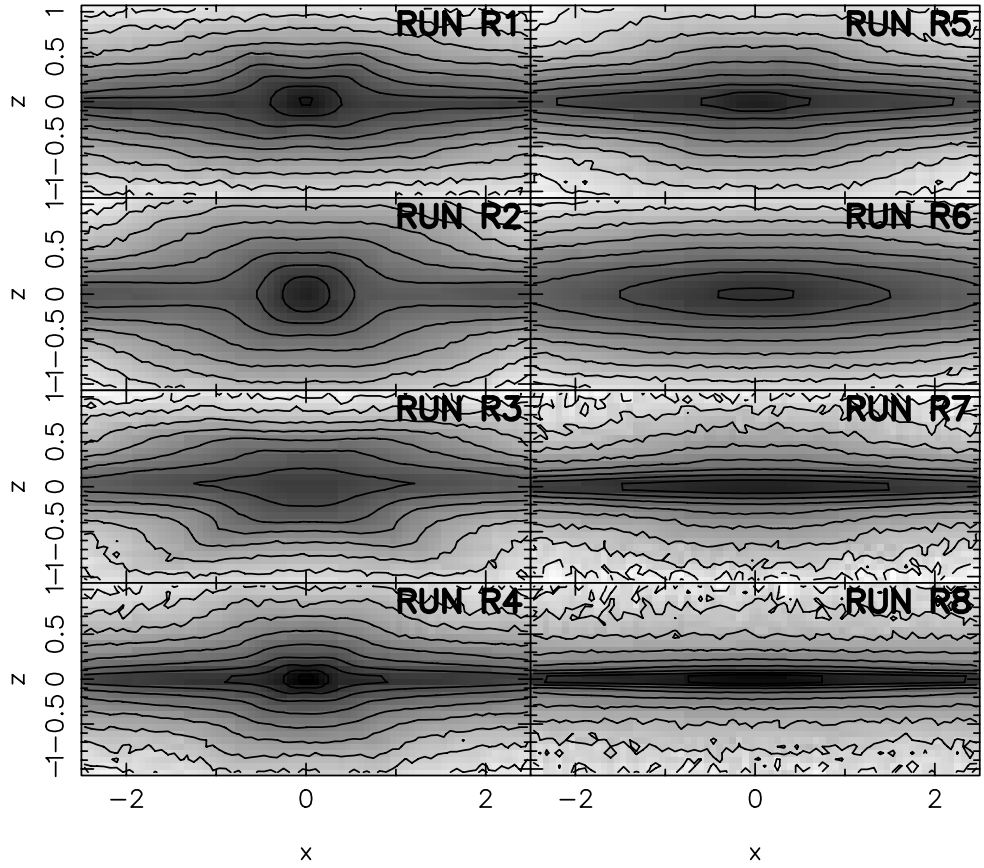

FIG. 3.—Edge-on view of runs R1–R8. In all cases, the bar has been rotated into the x-axis, so it is viewed side-on.

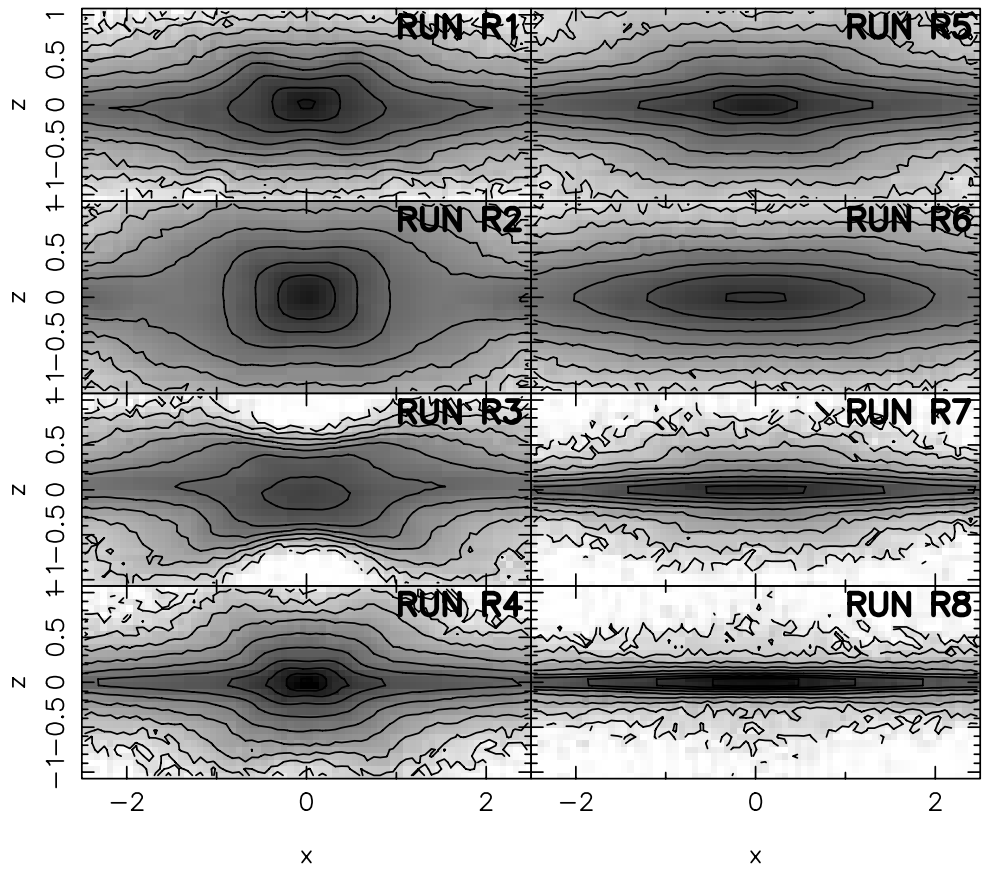

FIG. 4.—Edge-on view of the systems as in Fig. 3, but with only $|y| \leq 0.5$ shown.

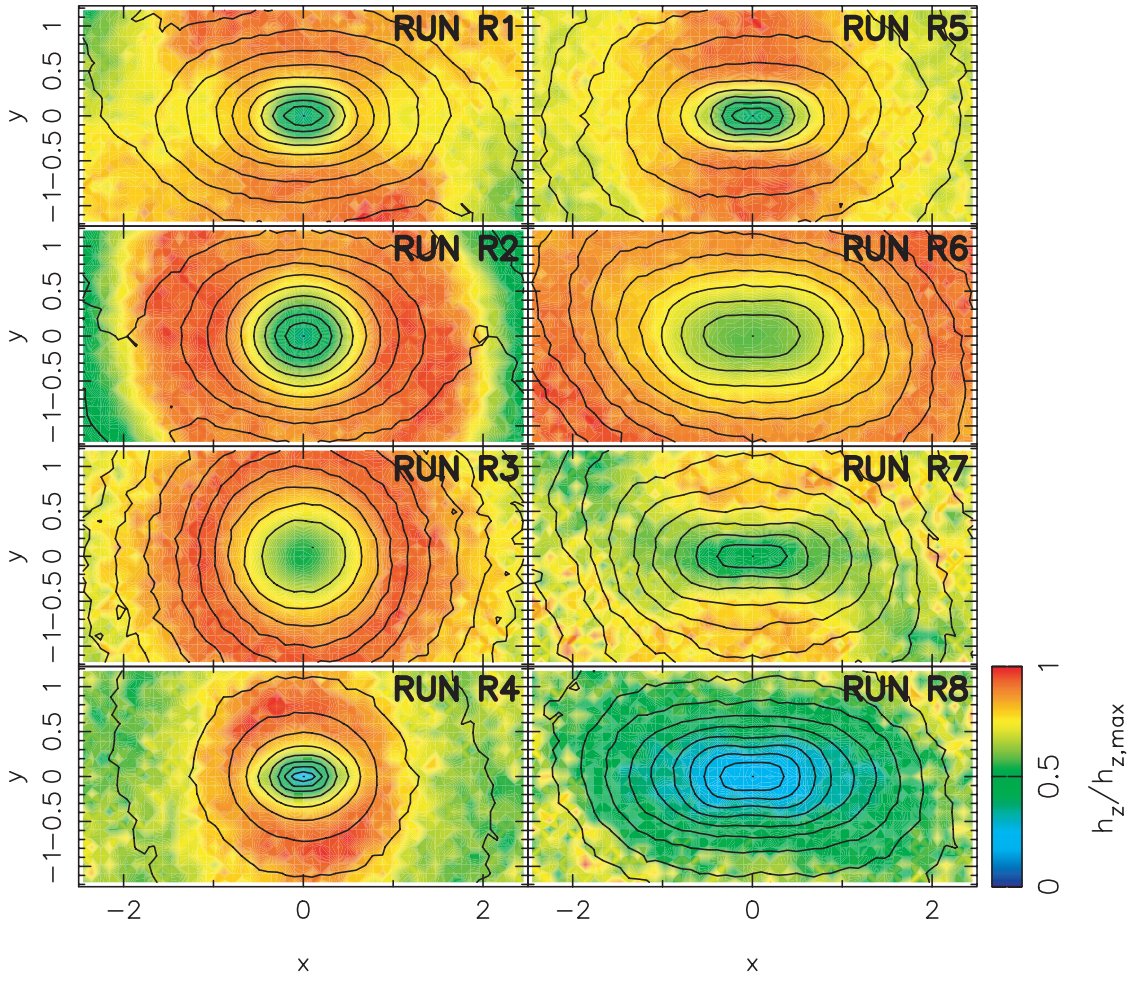

FIG. 5.—Face-on view of runs R1–R8 showing the color-coded rms height (h_z) of particles. The contours show the projected surface density Σ.

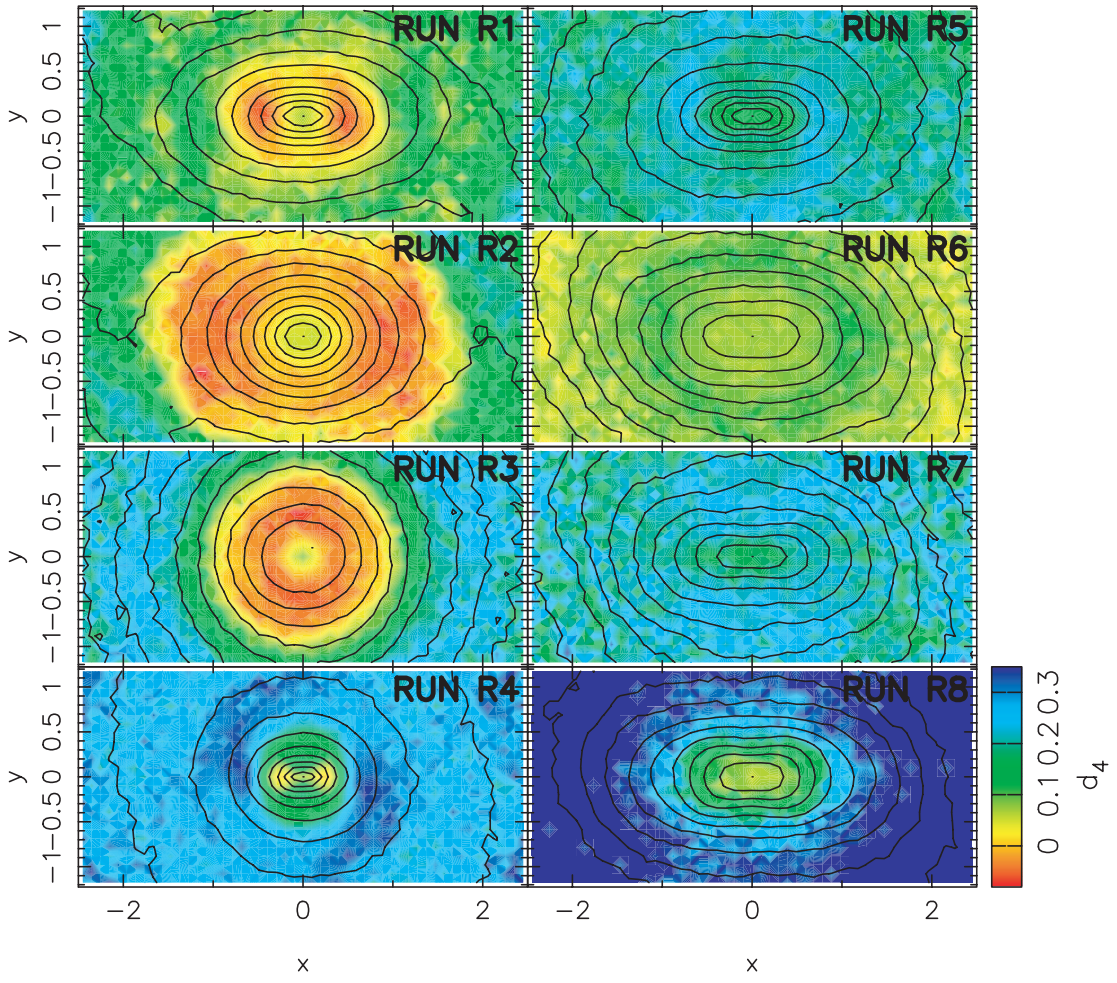

FIG. 6.—Face-on view of runs R1–R8 showing the fourth-order Gauss-Hermite moment of the vertical density distribution, d_4.

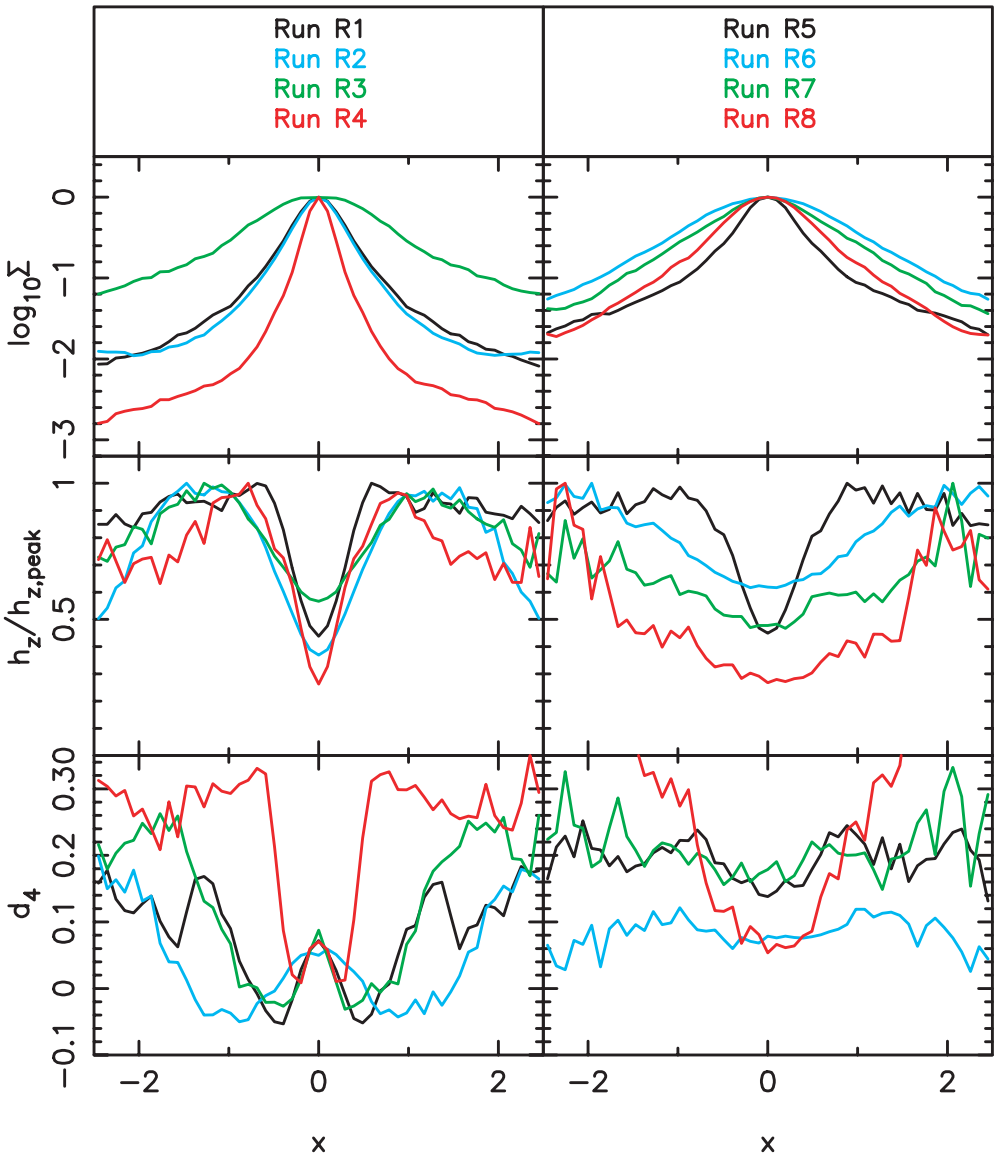

FIG. 7.—Summary of the face-on density moments along the bars' major axes for runs R1–R8.

For better comparison of the different models, Figure 7 shows the density, h_z, and d_4 profiles along the major axes of the face-on bars.

4.1. h_z *versus* d_4

Are the second and fourth density moments equivalent ways of defining the peanut? Figure 7 shows that the maxima in h_z corresponds very well to the minima in d_4 in runs R1 and R2. In run R3 the peak of h_z is at a different radius from the minimum of d_4, while in run R4 h_z and d_4 have *maxima* at about the same point. Thus the maximum in h_z and the minimum in d_4 are not equivalent ways of defining the peanut.

Which of h_z and d_4 is the better tracer of peanuts? Figure 7 shows that the major-axis h_z profiles of runs R1 and R5 are rather similar, suggesting very similar peanuts; Figures 3 and 4 show that this is far from being the case. In contrast, their d_4 profiles in Figure 7 are very different. For this reason d_4 is a better measure of the presence and strength of a peanut. The reason why h_z is not an optimal peanut diagnostic is that it is partly determined by the local projected density, as suggested by the correlation, evident in Figure 7, between the depth of the central minimum in h_z and the central concentration.

5. VERTICAL KINEMATICS OF PEANUTS

5.1. *The Absence of a Peanut Signature in* σ_z

Figure 8 shows maps of σ_z for runs R1–R8. No sign of the peanuts is evident in these maps. We found that in the region $-2.5 \leq x, y \leq 2.5$ of all the models, σ_z correlates very strongly with Σ, even off the bar's major axis. The signature of a peanut is buried in the small scatter in σ_z at fixed Σ, making the peanut hard to distinguish from σ_z.

5.2. *A Peanut Signature in* σ_z^2/Σ

Following the discussion in § 2, it is unsurprising that we cannot identify peanuts from σ_z profiles. Since $\sigma_z^2 \sim \Sigma$ in the isothermal disk (eq. [4]), it is worth exploring whether σ_z^2/Σ is better than σ_z at locating peanuts. In Figure 9 we plot, for runs R1–R8, σ_z^2/Σ on the bars' major axes. In all cases, the profiles of $\log(\sigma_z^2/\Sigma)$ are rather similar to those of h_z (although there is not a one-to-one correspondence). However, a comparison of Figures 7 and 9 shows that the minimum in d_4, which we showed above to be a good indicator of a peanut, does not correspond to any special point in the σ_z^2/Σ profile. Therefore σ_z^2/Σ has the same limitations as a peanut diagnostic as h_z, although it may

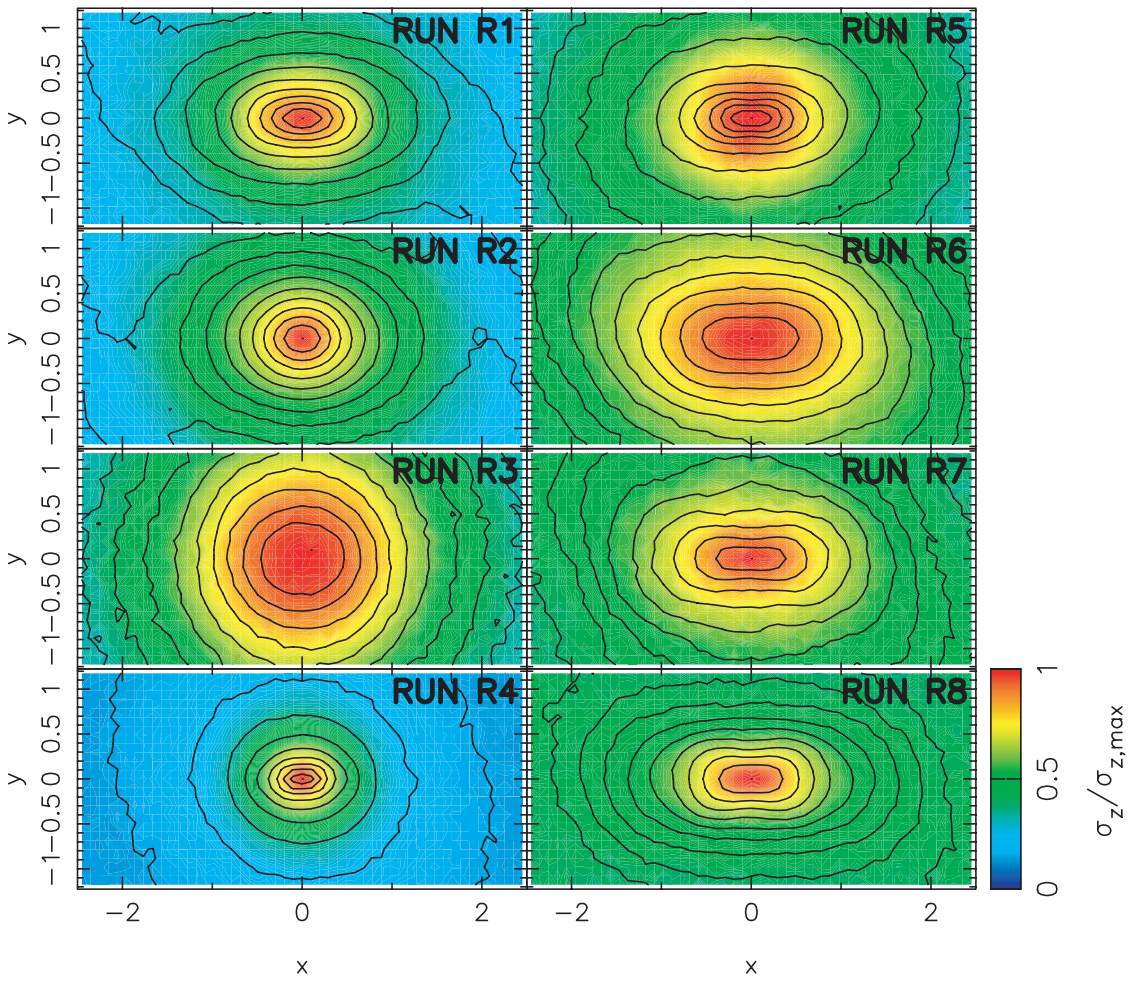

FIG. 8.—Face-on view of runs R1–R8 showing σ_z.

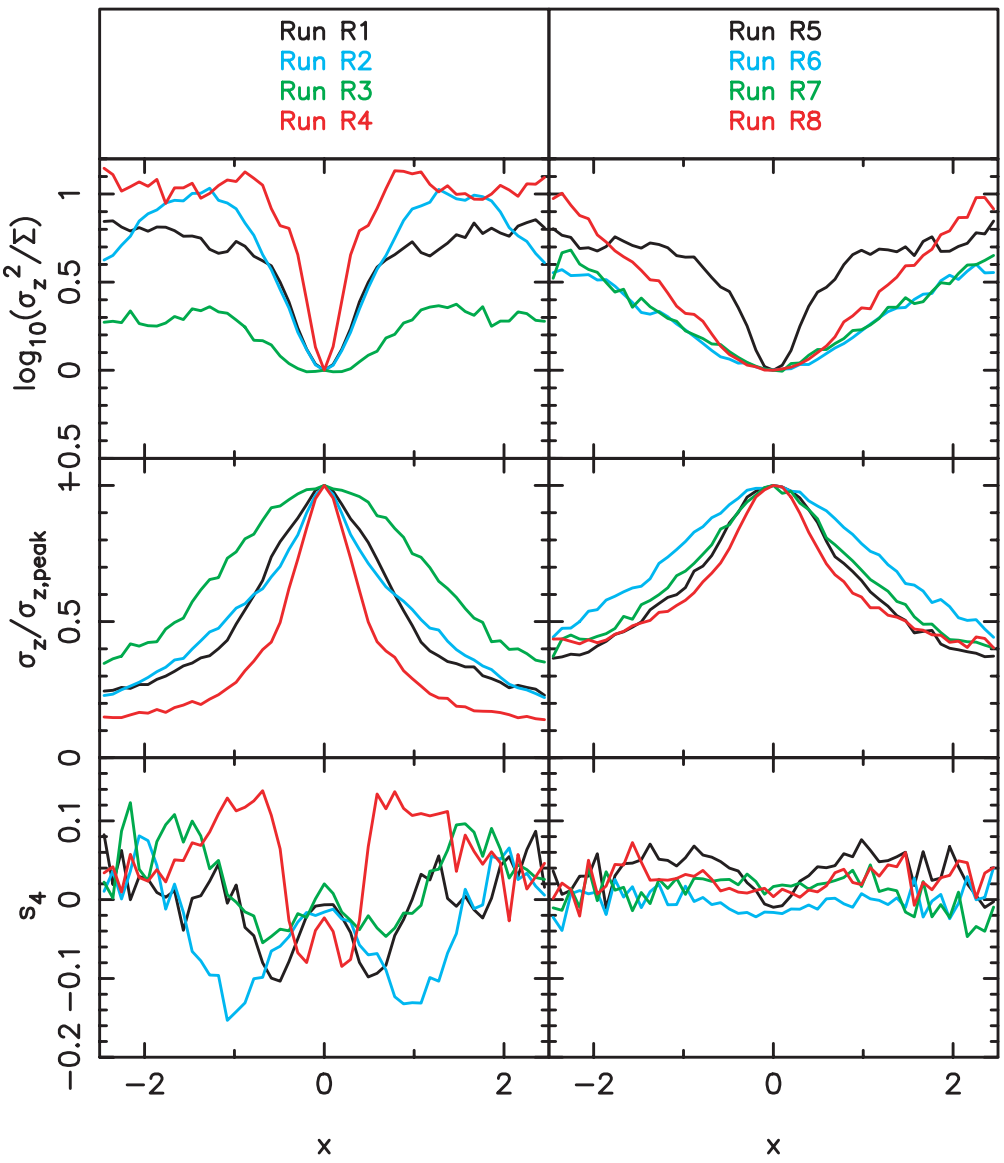

FIG. 9.—Summary of the face-on kinematic moments along the bars' major axes for runs R1–R8. The peanut is not apparent in the velocity dispersion profile but is prominent in the s_4 profile.

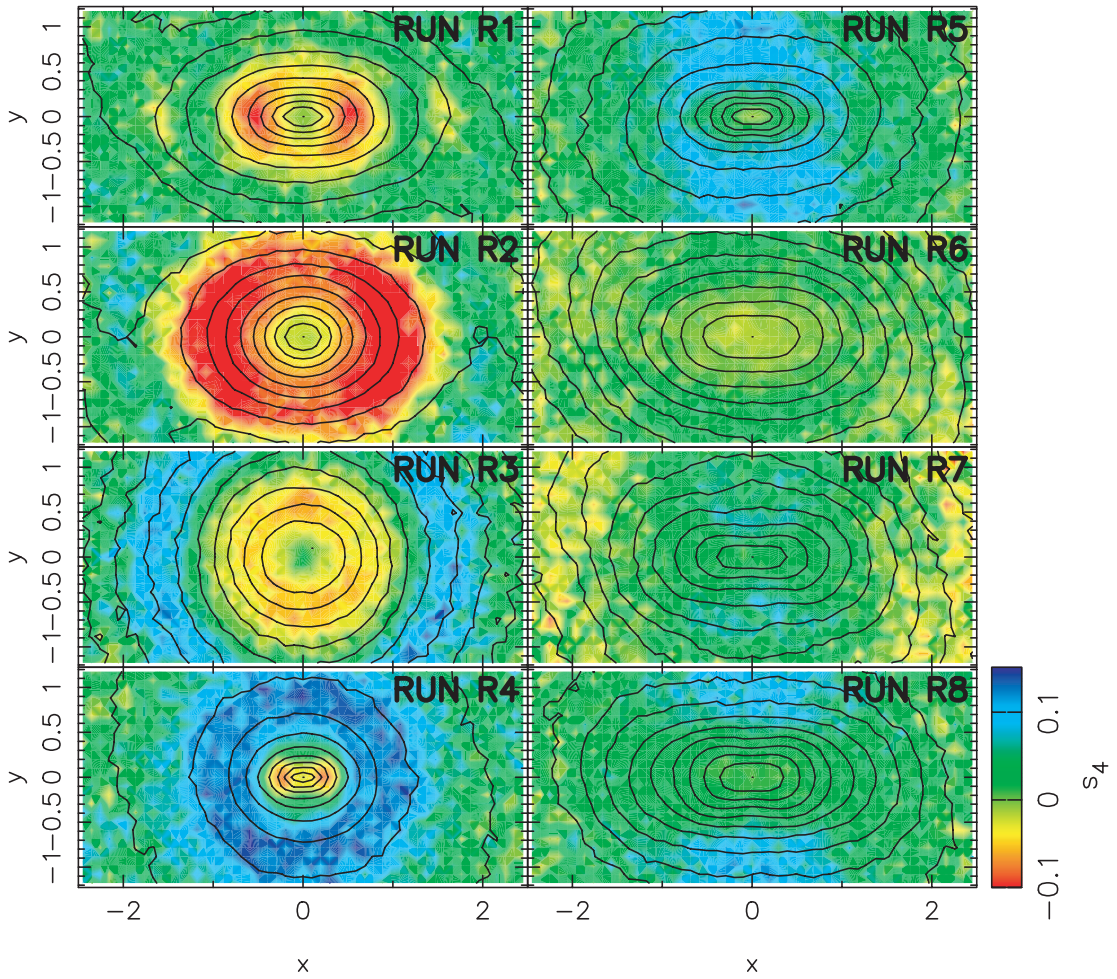

FIG. 10.—Face-on view of runs R1–R8 showing s_4.

still be useful in distinguishing between peanut and peanutless systems.

5.3. *The Peanut Signature in s_4*

Figure 10 plots s_4 for runs R1–R8. A qualitative difference between the peanut systems and the peanutless ones is evident: two negative minima at the location of the peanut on the bar's major axis if a peanut is present. In runs R1–R4 there is a considerable variation in bar strength, but in each case, the negative s_4 minimum criterion recognizes the peanut, demonstrating that it does not depend on bar strength.

In run R5, which produced a weak peanut, s_4 remains greater than zero on the bar's major axis, and the only minimum is at $R = 0$. Thus the kinematic diagnostic cannot identify weak peanuts. Other than at $R = 0$, no significantly negative minimum in s_4 occurs in runs R6–R8, which lack a peanut.

Figure 11 plots s_4 versus d_4 on the major axes of the bars. As predicted by the analytic models of § 2, the minimum in d_4, which is a tracer of the peanut, corresponds to the minimum of s_4. Therefore minima in s_4 are an excellent kinematic peanut diagnostic in these face-on systems.

5.4. *Live-Halo Simulation*

Mainly because of the lower mass resolution, which results in significantly lower S/N in the Gauss-Hermite moments, we used the live-halo run L1 only to confirm results of the rigid-halo simulations. Despite the lower S/N, we were still able to identify clear and well-matched minima in d_4 and s_4 in the region of the peanut. Indeed, the properties of the peanut in L1 are very similar to those in run R1, although the initial conditions, including vertical structure, were quite different. This gives us confidence that the peanut diagnostic developed from rigid-halo simulations is not an artifact of the rigid halos.

5.5. *Simulations with Bulges*

Now we consider simulations that include a bulge in the initial conditions. In Figure 12 we plot the edge-on views of these systems. A weak peanut is present in run B1, which is masked in the full edge-on view. A stronger peanut is present in run B2, and an even stronger one in B3. Comparing with Figures 3 and 4, the pure disk components of runs B1, B2, and B3 are most like runs R5, R4, and R1, respectively, albeit only approximately. Figure 13 plots maps of d_4 and s_4, and the major-axis profiles are presented in Figure 14. In all three runs, the slope of the profile of h_z has a break that allows the peanut to be recognized. Thus the peanuts are still evident in σ_z^2/Σ, including again the weak peanut in B1. All three models have minima in their d_4 profiles, but those in runs B1 and B2 are broad ones extending down to $R = 0$. In s_4, no minima are visible in run B1 (and thus no peanut is identified, as was the case also for the weak peanut in run R5), while the usual minima identifying a peanut are clear in run B3. The case of run B2 is

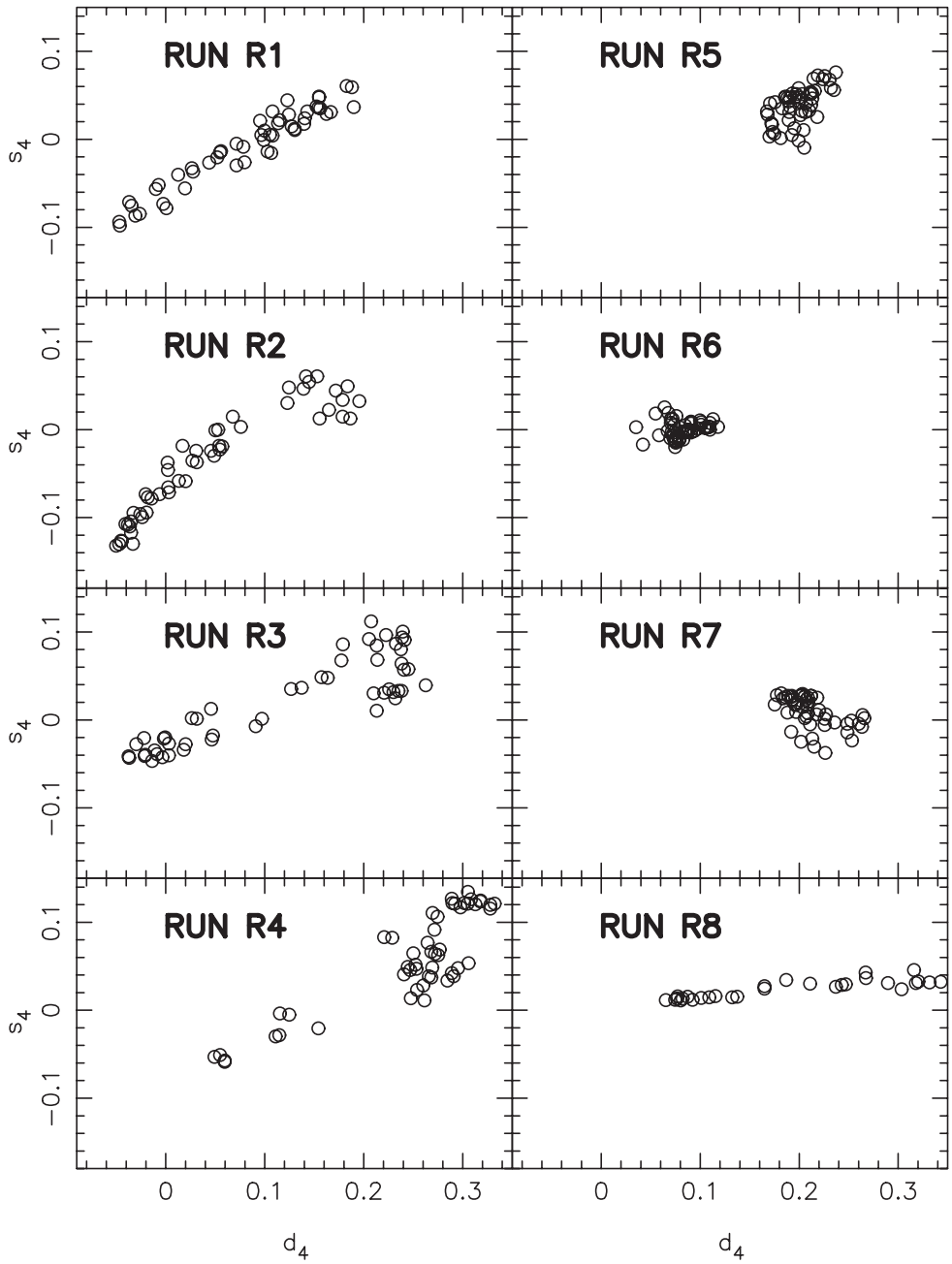

FIG. 11.—Variation of s_4 vs. d_4 on the bars' major axes for runs R1–R8.

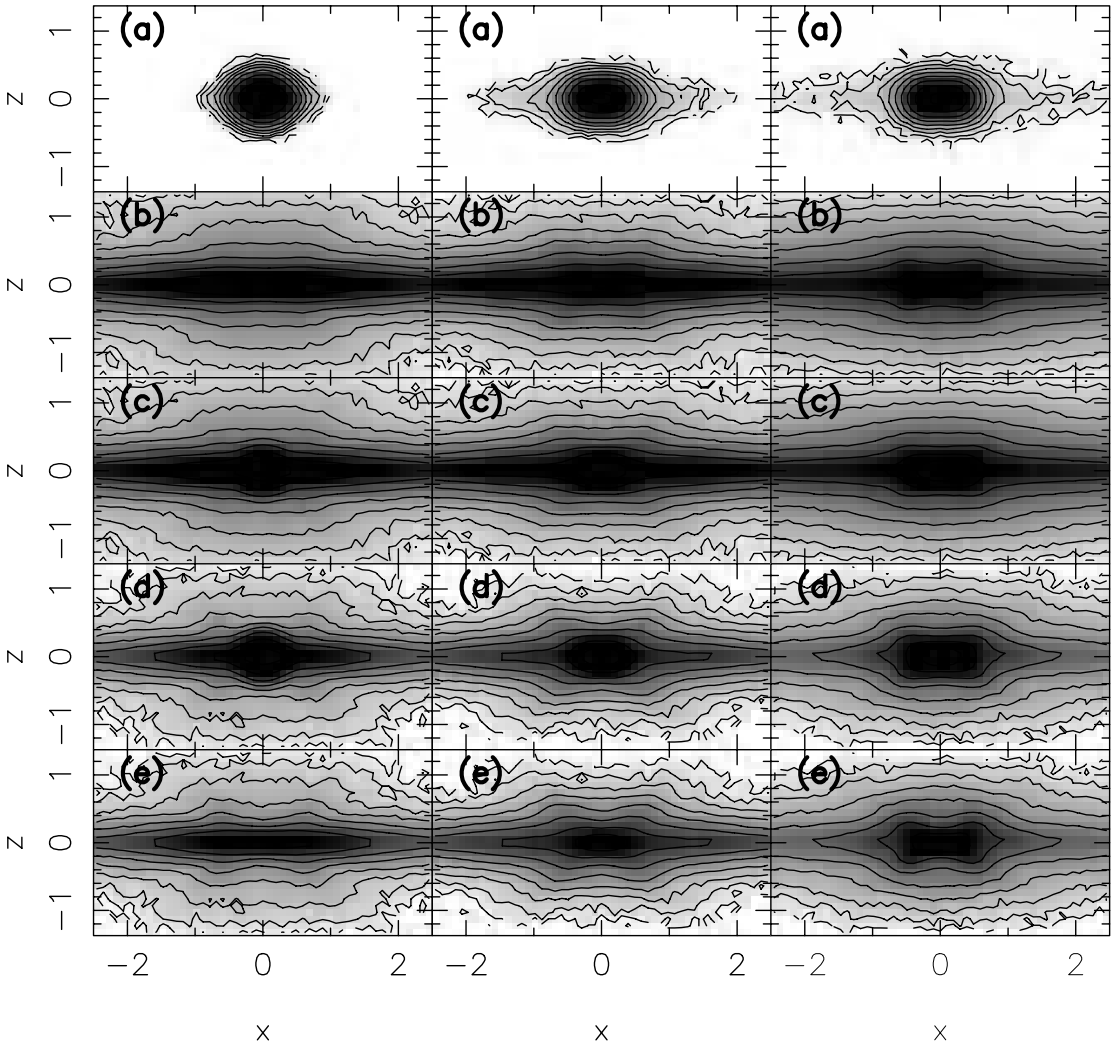

FIG. 12.—Disk+bulge simulations. *Left*, Run B1; *middle*, run B2, *right*, run B3. (*a*) Bulges; (*b*) disks; (*c*) bulges+disks; (*d*, *e*) bulges+disks and disks in the range $|y| \leq 0.5$.

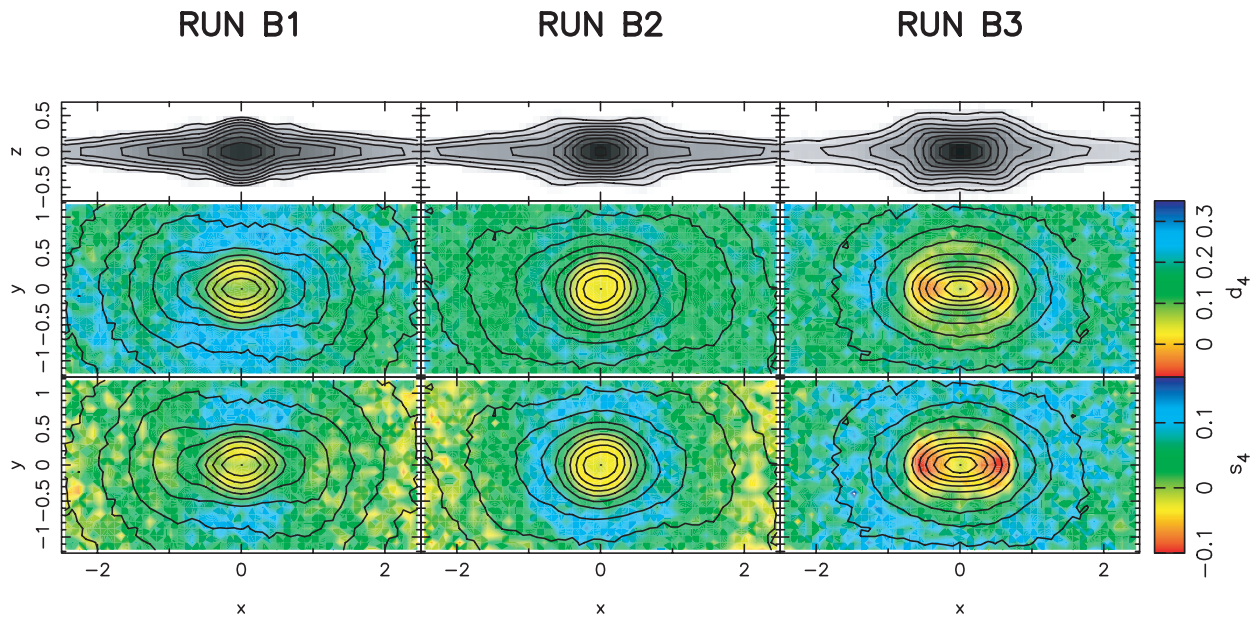

FIG. 13.—Bulge simulations B1–B3. [*The bottom left and bottom right panels are available as mpeg files in the electronic edition of the Journal, showing the effect of inclination.*]

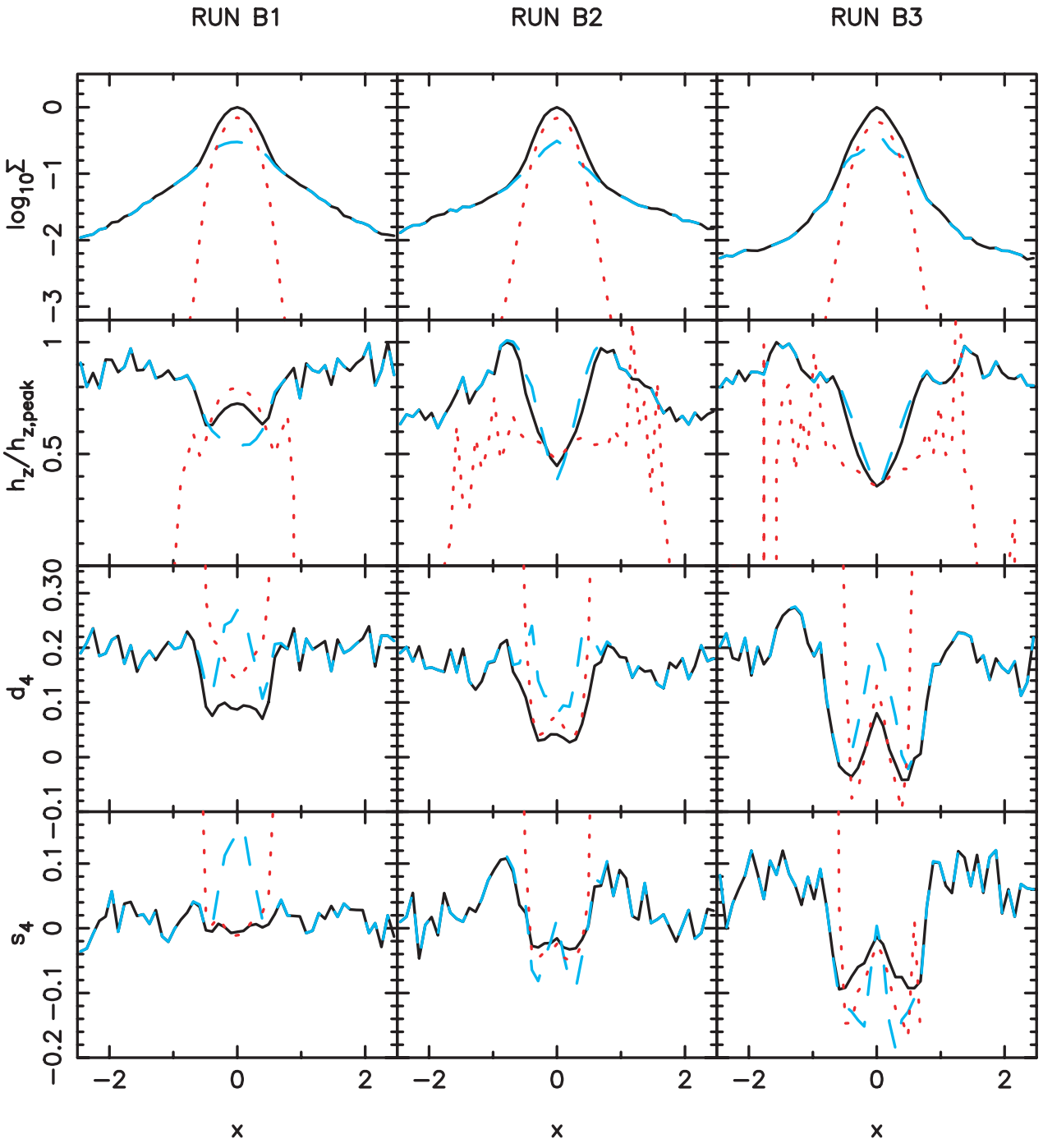

FIG. 14.—Photometric profiles of runs B1–B3 on the bars' major axes. The red dotted line is for the bulge, the cyan dashed line is for the disk, and the black solid line is for disk+bulge.

more interesting. If the bulge in this system were dark, a peanut would stand out clearly in s_4 (*cyan line*); with the addition of the bulge, the different bulge kinematics, especially the significantly higher σ_z, perturb the net s_4, hiding the presence of a peanut in the sense that only a single broad minimum down to $R = 0$ remains in its profile.

6. THE EFFECT OF INCLINATION

Exactly face-on galaxies are rare; the probability of a galaxy being within 5° of edge-on is over 20 times larger than that of its being within 5° of face-on (8.7% vs. 0.4%). The inclination needs to be within 24° of face-on before its probability is equal to that of its being 5° from edge-on. A sample of exactly face-on galaxies may therefore be hard to obtain. Thus it is necessary to ask what happens to the kinematic signature of a peanut when it is viewed not quite perfectly face-on. Is it possible that the negative minimum in the s_4 signature of a peanut is erased, or induced where no peanut is present, for other than an exactly face-on orientation?

Once a system is no longer perfectly face-on, the observed LOS velocity dispersion $\sigma_{\rm los}$ relative to which s_4 is defined includes contributions from the radial (σ_R) and tangential (σ_ϕ) dispersion components. If i is the inclination angle, ϕ is any angle in the disk's plane measured relative to the inclination

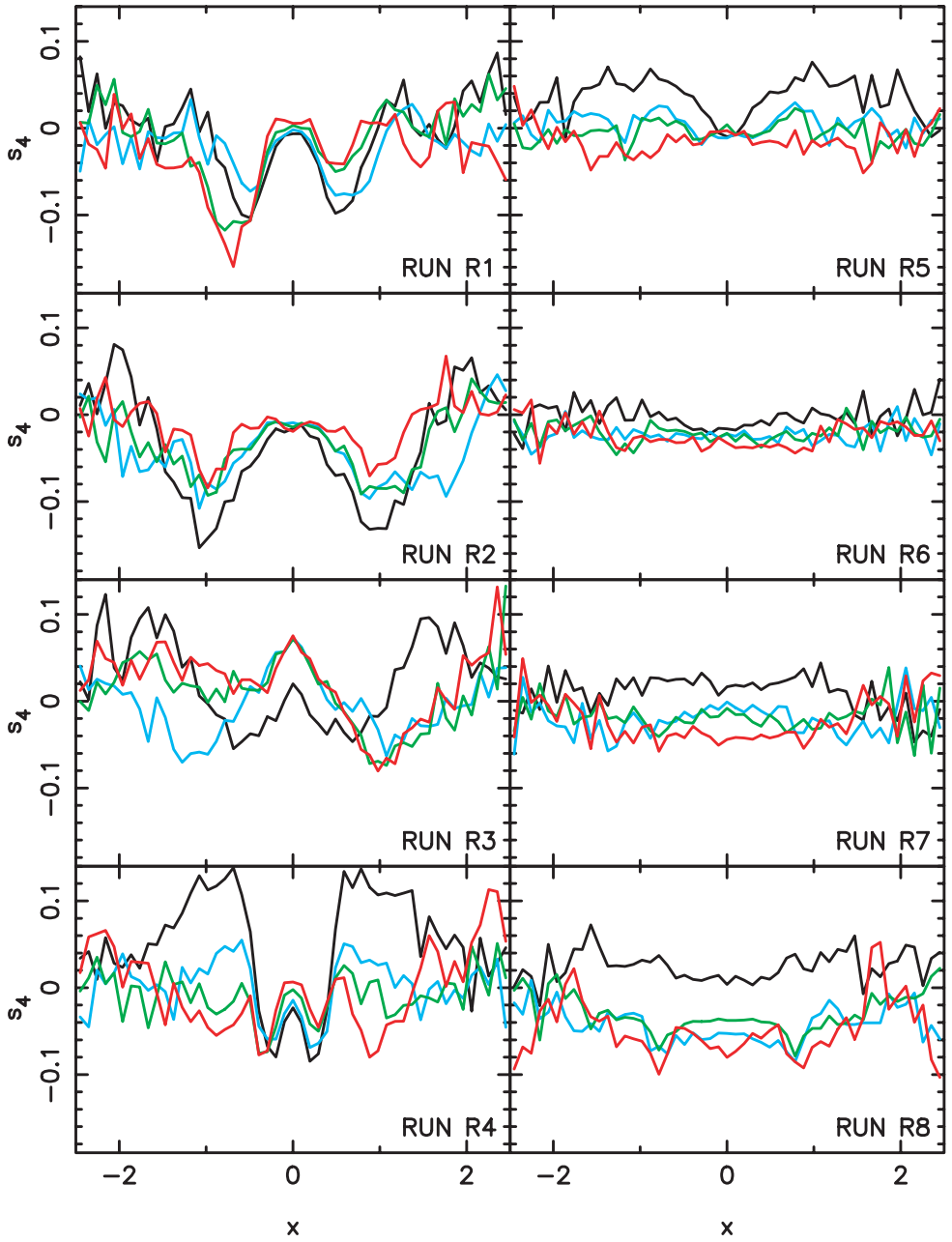

FIG. 15.—The s_4 profiles on the bar's major axis seen face-on (*black line*) and at $i = 30^\circ$ for runs R1–R8. The bar makes an angle of $\phi = 0^\circ$, 45°, and 90° for the cyan, green, and red lines, respectively. In our notation, $x > 0$ is the side nearer the observer.

axis, $\alpha \equiv \sigma_\phi/\sigma_R$, and $\beta \equiv \sigma_z/\sigma_R$, then the contribution of σ_z to $\sigma_{\rm los}$ is

$$\left(\frac{\sigma_z}{\sigma_{\rm los}}\right)^2 = \frac{1}{\beta^{-2}\sin^2\phi\sin^2 i + \alpha^2\beta^{-2}\cos^2\phi\sin^2 i + \cos^2 i}. \quad (11)$$

This has a maximum along the disk's major axis ($\phi = 0$) and a minimum on the minor axis ($\phi = 90^\circ$). A crude estimate of $\sigma_z/\sigma_{\rm los}$ can be obtained assuming that $\alpha^2 = \frac{1}{2}$ (i.e., a flat rotation curve). Then if $\beta = 0.293$ (the minimum value required for stability [Araki 1985]), we estimate that the contamination may be as high as 10% already at an inclination of 10°. However, $\beta = 0.293$ is extreme; in the solar neighborhood, Dehnen & Binney (1998) find $\beta = 0.53 \pm 0.07$, while Gerssen et al. (2000) find even larger β-values in earlier Hubble types. The contamination of σ_z in $\sigma_{\rm los}$ is still less than 10% at $i = 30^\circ$ on the disk's major axis if $\beta = 0.53$.

Since these estimates are based on simplifying approximations, we also explored the effect of inclination directly on the N-body simulations to $i = 40^\circ$. Figure 15 presents s_4 on the bar's major axis for runs R1–R8 inclined at $i = 30^\circ$ and with the bar oriented at $0^\circ \le \phi \le 90^\circ$.

For strong peanuts, the negative s_4 minimum criterion still distinguishes between peanut and peanutless systems up to an inclination of $\sim 30^\circ$. When a peanut is present, the two minima on opposite sides of the bar become asymmetric as ϕ increases to 90°. Therefore $\phi \lesssim 45^\circ$ is a more favorable orientation for finding peanuts. In some instances, inclination produces negative minima in s_4 off the bar's major axis in both peanut and peanutless systems. However, inclination leads to, at most, only shallow minima in peanutless systems, although an overall

negative s_4 can result when no peanut is present. (Thus a negative s_4 without a minimum is not by itself sufficient as a peanut diagnostic.)

In run R8 we prevented bending by forcing mid-plane symmetry, which resulted in a final $\sigma_z/\sigma_R \simeq 0.25$. When this system is viewed at an inclination of 30°, two *shallow* minima in s_4 appear at all ϕ (see Fig. 15), even though no peanut is present. As expected from the analytic estimate above, inclination has a much larger effect on the vertical kinematic moments of vertically cold systems. As this is an unrealistically anisotropic system (symmetrization about the disk plane having inhibited the bending instability), this simulation represents an extreme extent to which inclination introduces minima in s_4 when no peanut is present.

Two animations accompany the online version of Figure 13. These show the effect of inclination on the s_4 moments of simulations B1 and B3.

7. OBSERVATIONAL REQUIREMENTS

Measuring kinematic Gauss-Hermite moments requires high-S/N spectra (Bender et al. 1994). In our *N*-body measurements, this has been possible because of the large number of particles. By resampling experiments, we determined that S/N $\gtrsim 50$ is required to measure s_4 sufficiently accurately to identify a peanut, in good agreement with Bender et al. (1994). Fortunately, bars are generally bright features, which helps improve the S/N.

The kinematic signature of a peanut is strong for some distance on the bar's minor axis (Fig. 10). Thus very precise placement of the slit along the bar's major axis is not necessary. This also allows the widest slit consistent with the necessary spectral resolution.

The spectral resolution, R, required depends on the value of σ_z, which varies from galaxy to galaxy. The Milky Way has $\sigma_z \sim 100$ km s^{-1} (Kuijken 2003). Thus one would need R $\simeq$ 2500 to find a peanut in a face-on galaxy like the Milky Way. If, on the other hand, $\sigma_z \sim 30$ km s^{-1} (e.g., Bottema 1993), R $\simeq$ 8500 would be needed.

8. DISCUSSION

B/P-shaped bulges are common in edge-on disks, and simulations show that these can form by secular evolution in barred galaxies. In this paper we have explored the signature of peanuts on the vertical density and the resulting kinematics. We have shown that both h_z and d_4 are affected by a peanut, but the two are not equivalent signatures of a peanut. The preferred peanut signifier is d_4 since it distinguishes between weak and strong peanuts.

The vertical velocity dispersion σ_z is a poor diagnostic for peanuts because it depends on the local density. The quantity σ_z^2/Σ, which in an isothermal disk would trace h_z, factors out some of this dependence and is able to identify peanuts, even weak ones, at breaks in its slope. However, it is unable to quantify peanut strength and correlates poorly with d_4. This parameter may also be prone to systematic effects from variations in mass-to-light ratios if, for example, the bulge and the disk are composed of different stellar populations, as would happen if the bulge formed at high redshift through mergers. Nevertheless, this is a useful peanut diagnostic that is worth testing in real galaxies.

An excellent kinematic diagnostic of face-on peanuts is negative double minima in the Gauss-Hermite moment s_4. The negative s_4 minimum signature of a peanut holds for any bar strength down to the weakest of ovals and may therefore be used to search also for peanuts in unbarred galaxies. This diagnostic is not too sensitive to inclination for $i < 30°$, with negative minima on a bar's major axis continuing to be associated with the presence of a peanut. However, inclination leads to an asymmetry between the two sides of the bar as the bar orientation approaches the minor axis. Thus a bar oriented within ~45° of the line of nodes is ideal for a peanut search.

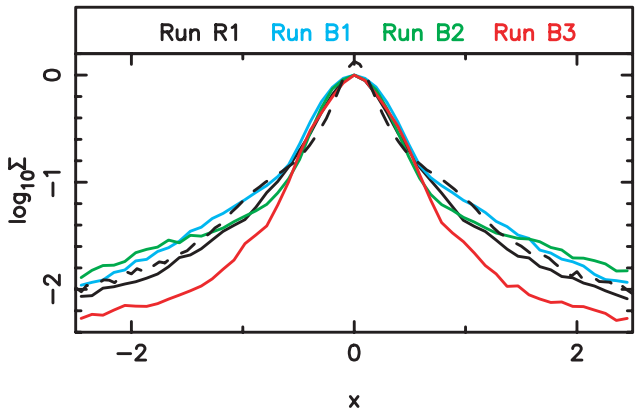

FIG. 16.—Comparison of the density profiles along the bars' major axes in runs R1 and B1–B3. The central concentration is largely due to initial conditions in runs B1–B3 but results from secular evolution in run R1. The dashed black line shows the scaled profile along the bar's major axis in NGC 4477.

8.1. *Bulge Formation Mechanisms and Vertical Structure*

Two competing models of bulge formation—via internal secular evolution and via external drivers—each account for a significant body of observational evidence, suggesting that both processes play some role (e.g., Wyse 2004). Thus we need to ask which process dominates in which galaxies. The results here suggest a novel observational program to address this question by targeting the degree of decoupling of the vertical structure of bulges and bars. To be concrete, consider runs R4 and B2, both of which contain a peanut. Since the bulge is already present in the initial conditions in run B2 (as would be a bulge formed in an early merger), the presence of a peanut cannot be used to address whether the bulge formed by secular evolution or not. Photometrically the two have similar density profiles (Fig. 16) since run R1 acquired a central density concentration by secular evolution (Hohl 1971; Debattista et al. 2004). These profiles are typical of the major-axis profiles of real galaxies: the dashed line in this figure shows the *J*-band profile of the nearly face-on galaxy NGC 4477, taken from the online[3] Frei catalog of galaxies (Frei et al. 1996). However, the vertical structure of the bulge in run B2 is qualitatively different from that in run R1 because it is not derived from the disk's vertical structure. Because of this, neither the d_4 nor the s_4 profiles have the kind of separated minima associated with peanuts in which the central concentration forms purely by secular evolution. Peanuts have been shown to be visible in 45% of edge-on galaxies, which means that they are even more common since projection hides some fraction of peanuts. Thus a kinematic survey of face-on barred galaxies should turn up a large fraction of galaxies with the negative s_4 minima signature of a peanut if bulges are built largely by secular evolution of bars. On the other hand, if bulges formed largely through mergers of

[3] Available at http://www.astro.princeton.edu/~frei/catalog.htm.

dwarfs, then peanuts would need to be stronger to be identifiable in face-on kinematics.

8.2. *The Effect of Gas*

The simulations presented here were all collisionless. If gas funneled by a bar plays an important role also in bulge formation, naively it would seem likely that the vertical kinematic signature of a peanut becomes confused. However, in a barred potential gas sinks to small radii, where its kinematics and that of stars formed from it do not perturb those from the peanut farther out. Lower resolution hydro+*N*-body live-halo experiments that we have run and that will be presented elsewhere show that peanuts can still be recognized in this case with the same stellar kinematic diagnostic. Therefore, an observational survey of face-on barred galaxies to look for peanuts appears worth undertaking.

We would like to thank the anonymous referee for comments that helped improve the presentation of this paper. V. P. D. thanks Enrico Maria Corsini, Sven De Rijcke, and Ortwin Gerhard for fruitful discussion.

REFERENCES

Andredakis, Y. C., & Sanders, R. H. 1994, MNRAS, 267, 283
Araki, S. 1985, Ph.D. thesis, MIT
Athanassoula, E. 2005, MNRAS, 358, 1477
Athanassoula, E., & Bureau, M. 1999, ApJ, 522, 699
Bender, R., Saglia, R. P., & Gerhard, O. E. 1994, MNRAS, 269, 785
Bettoni, D., & Galletta, G. 1994, A&A, 281, 1
Binney, J., & Petrou, M. 1985, MNRAS, 214, 449
Binney, J., & Tremaine, S. 1987, Galactic Dynamics (Princeton: Princeton Univ. Press)
Bissantz, N., Debattista, V. P., & Gerhard, O. 2004, ApJ, 601, L155
Böker, T., Stanek, R., & van der Marel, R. P. 2003, AJ, 125, 1073
Bottema, R. 1993, A&A, 275, 16
Burbidge, E. M., & Burbidge, G. R. C. 1959, ApJ, 130, 20
Bureau, M., & Athanassoula, E. 1999, ApJ, 522, 686
———. 2005, ApJ, 626, 159
Bureau, M., & Freeman, K. C. 1999, AJ, 118, 126
Camm, G. L. 1950, MNRAS, 110, 305
Carollo, C. M. 1999, ApJ, 523, 566
Carollo, C. M., Stiavelli, M., de Zeeuw, P. T., Seigar, M., & Dejonghe, H. 2001, ApJ, 546, 216
Carollo, C. M., Stiavelli, M., & Mack, J. 1998, AJ, 116, 68
Chung, A., & Bureau, M. 2004, AJ, 127, 3192
Combes, F., Debbasch, F., Friedli, D., & Pfenniger, D. 1990, A&A, 233, 82
Combes, F., & Sanders, R. H. 1981, A&A, 96, 164
Courteau, S., de Jong, R. S., & Broeils, A. H. 1996, ApJ, 457, L73
Debattista, V. P. 2003, MNRAS, 342, 1194
Debattista, V. P., Carollo, C. M., Mayer, L., Moore, B. 2004, ApJ, 604, L93
Debattista, V. P., & Sellwood, J. A. 2000, ApJ, 543, 704
de Carvalho, R. R., & da Costa, L. N. 1987, A&A, 171, 66
de Grijs, R., & Peletier, R. F. 1997, A&A, 320, L21
Dehnen, W., & Binney, J. 1998, MNRAS, 298, 387
de Jong, R. S. 1996, A&A, 313, 45
Eskridge, P. B., et al. 2000, AJ, 119, 536
Ferreras, I., Wyse, R. F. G., & Silk, J. 2003, MNRAS, 345, 1381
Frei, Z., Guhathakurta, P., Gunn, J. E., & Tyson, J. T. 1996, AJ, 111, 174
Fukugita, M., Hogan, C. J., & Peebles, P. J. E. 1998, ApJ, 503, 518
Gerhard, O. E. 1993, MNRAS, 265, 213
Gerssen, J., Kuijken, K., & Merrifield, M. R. 2000, MNRAS, 317, 545
Hernquist, L. 1990, ApJ, 356, 359
———. 1993, ApJS, 86, 389
Hohl, F. 1971, ApJ, 168, 343
Jarvis, B. J. 1986, AJ, 91, 65
Kauffmann, G., White, S. D. M., & Guiderdoni, B. 1993, MNRAS, 264, 201
Knapen, J. H., Shlosman, I., & Peletier, R. F. 2000, ApJ, 529, 93
Kormendy, J. 1993, in IAU Symp. 153, Galactic Bulges, ed. H. Dejonghe & H. J. Habing (Dordrecht: Kluwer), 209
Kormendy, J., Bender, R., & Bower, G. 2002, in ASP Conf. Ser. 273, The Dynamics, Structure, and History of Galaxies, ed. G. S. Da Costa & H. Jerjen (San Francisco: ASP), 29
Kormendy, J., & Illingworth, G. 1982, ApJ, 256, 460
Kormendy, J., & Kennicutt, R. 2004, ARA&A, 42, 603
Kuijken, K. 2003, preprint (astro-ph/0310903)
Kuijken, K., & Merrifield, M. R. 1995, ApJ, 443, L13
Lütticke, R., Dettmar, R.-J., & Pohlen, M. 2000, A&AS, 145, 405
Lütticke, R., Pohlen, M., & Dettmar, R.-J. 2004, A&A, 417, 527
MacArthur, L. A., Courteau, S., & Holtzman, J. A. 2003, ApJ, 582, 689
Merrifield, M. R., & Kuijken, K. 1999, A&A, 345, L47
Merritt, D., & Sellwood, J. A. 1994, ApJ, 425, 551
Navarro, J. F., Frenk, C. S., & White, S. D. M. 1996, ApJ, 462, 563
Patsis, P. A., Athanassoula, E., Grosbøl, P., & Skokos, Ch. 2002a, MNRAS, 335, 1049
Patsis, P. A., Skokos, Ch., & Athanassoula, E. 2002b, MNRAS, 337, 578
Peletier, R. F., & Balcells, M. 1996, AJ, 111, 2238
Persic, M., & Salucci, P. 1992, MNRAS, 258, 14P
Pfenniger, D. 1984, A&A, 134, 373
———. 1985, A&A, 150, 112
Pfenniger, D., & Friedli, D. 1991, A&A, 252, 75
Pizzella, A., Corsini, E. M., Vega Beltrán, J. C., & Bertola, F. 2004, A&A, 424, 447
Prendergast, K. H., & Tomer, E. 1970, AJ, 75, 674
Quillen, A. C., Kuchinski, L. E., Frogel, J. A., & Depoy, D. L. 1997, ApJ, 481, 179
Raha, N., Sellwood, J. A., James, R. A., & Kahn, F. D. 1991, Nature, 352, 411
Sellwood, J. A., & Valluri, M. 1997, MNRAS, 287, 124
Shaw, M. A. 1987, MNRAS, 229, 691
Spitzer, L., Jr. 1942, ApJ, 95, 329
Springel, V., & White, S. D. M. 1999, MNRAS, 307, 162
Stadel, J. 2001, Ph.D. thesis, Univ. Washington
Stephens, A. W., et al. 2003, AJ, 125, 2473
Terndrup, D. M., Davies, R. L., Frogel, J. A., DePoy, D. L., & Wells, L. A. 1994, ApJ, 432, 518
van den Bosch, F. C., Abel, T., Croft, R. A. C., Hernquist, L., & White, S. D. M. 2002, ApJ, 576, 21
van der Kruit, P. C., & Freeman, K. 1986, ApJ, 303, 556
van der Kruit, P. C., & Searle, L. 1981, A&A, 95, 105
van der Marel, R. P., & Franx, M. 1993, ApJ, 407, 525
Whitmore, B. C., & Bell, M. 1988, ApJ, 324, 741
Wyse, R. F. G. 2004, ApJ, 612, L17
Zoccali, M., et al. 2003, A&A, 399, 931